Inorg. Chem. **2006**, *45*, 4637−4641

Crystal Growth, Structure, Magnetic, and Transport Properties of $TbRhIn_5$

Willa M. Williams,[†] Long Pham,[‡] Samuel MaQuilon,[‡] Monica Moldovan,[§] Zachary Fisk,[‡] David P. Young,[§] and Julia Y. Chan*,[†]

Departments of Chemistry and Physics and Astronomy, Louisiana State University, Baton Rouge, Louisiana 70803, and Department of Physics, University of California, Davis, California 95616

Received February 1, 2006

Single crystals of $TbRhIn_5$ were synthesized using the flux growth method. $TbRhIn_5$ adopts the $HoCoGa_5$ structure type and crystallizes in the space group *P*4/*mmm*, $Z = 1$. Lattice parameters are $a = 4.6000(6)$ Å, $c = 7.4370(11)$ Å, and $V = 157.29(6)$ Å^3. Transport measurements show that $TbRhIn_5$ is metallic ($d\rho/dT > 0$). A sharp antiferromagnetic transition is observed at $T_N = 48$ K in the susceptibility data for $TbRhIn_5$, which is highly anisotropic when the field is oriented along the *c* axis and *a*–*b* plane of the crystal and has an average effective moment of 9.72 μ_B/Tb^{3+}.

Introduction

Heavy fermion intermetallic compounds exhibit exotic physical properties caused by the interactions between their f electrons and conduction electrons.[1−10] Heavy fermions show normal metallic behavior at room temperature, while at lower temperatures, the conduction electrons begin to screen the magnetic moment, resulting in effective masses approximately 2 orders of magnitude higher than that of a free electron. Since the effective mass of an electron is proportional to the electronic specific heat (γ), a large Sommerfeld coefficient (>100 mJ/mol K^2) may be observed.[2] Recently, these compounds have been reviewed and summarized.[11] Heavy fermion compounds are typically cerium-, ytterbium-, or uranium-based intermetallic compounds.[5,12−14] The rare earth ions in intermetallic compounds are well separated, so that any direct exchange between two neighboring f shells is negligible.[15,16] Because of their metallic nature, however, the magnetic interaction between two such ions can take place via the polarization of the conduction band electrons, as in the case of the elemental rare-earth metals. This Ruderman−Kittel−Kasuya−Yoshida (RKKY) indirect exchange interaction is responsible for cooperative magnetic ordering.[15] The competition between Ruderman−Kittel−Kasuya−Yoshida (RKKY) interactions and the Kondo effect (the progressive screening of the magnetic moments by the conduction electrons at low temperatures) is important because the heavy fermion state is formed when the Kondo effect overcomes the RKKY interaction.[17]

$CeMIn_5$ (M = Co, Rh, Ir) is a special class of heavy fermion materials which show magnetic ordering and unconventional superconductivity at low temperatures.[18,19]

* To whom correspondence should be addressed. E-mail: jchan@lsu.edu. Phone: (225) 578-2695. Fax: (225) 578-3458.
[†] Department of Chemistry, Louisiana State University.
[‡] Department of Physics, University of California−Davis.
[§] Department of Physics and Astronomy, Louisiana State University.

(1) Fisk, Z.; Hess, D. W.; Pethick, C. J.; Pines, D.; Smith, J. L.; Thompson, J. D.; Willis, J. O. *Science* **1988**, *239*, 33−42.
(2) Fisk, Z.; Ott, H. R.; Rice, T. M.; Smith, J. L. *Nature* **1986**, *320*, 124−129.
(3) Movshovich, R.; Jaime, M.; Thompson, J. D.; Petrovic, C.; Fisk, Z.; Pagliuso, P. G.; Sarrao, J. L. *Phys. Rev. Lett.* **2001**, *86*, 5152−5155.
(4) Moshopoulou, E. G.; Sarrao, J. L.; Pagliuso, P. G.; Moreno, N. O.; Thompson, J. D.; Fisk, Z.; Ibberson, R. M. *Appl. Phys. A* **2002**, *74*, S895−S897.
(5) Steglich, F. *Phys. Rev. Lett.* **1979**, *43*, 1892−1896.
(6) Fisher, R. A.; Kim, S.; Woodfield, B. F.; Phillips, E.; Taillefer, L.; Hasselbach, K.; Flouquet, J.; Giorgi, A. L.; Smith, J. L. *Phys. Rev. Lett.* **1989**, *62*, 1411−1414.
(7) Pagliuso, P. G.; Thompson, J. D.; Hundley, M. F.; Sarrao, J. L.; Fisk, Z. *Phys. Rev. B* **2001**, *63*, 054426.
(8) Fisk, Z.; Sarrao, J. L.; Thompson, J. D. *Curr. Opin. Solid State Mater. Sci.* **1996**, *1*, 42−46.
(9) Fisk, Z.; Sarrao, J. L.; Thompson, J. D. *Proc. Natl. Acad. Sci.* **1995**, *92*, 6663−6667.
(10) Stewart, G. R. *Rev. Mod. Phys.* **1984**, *56*, 755−787.
(11) Thomas, E. L. T.; Millican, J. M.; Okudzeto, E. K.; Chan, J. Y. *Comments Inorg. Chem.* **2006**, *27*, 1−39.
(12) Ott, H. R.; Rudigier, H.; Fisk, Z.; Smith, J. L. *Phys. Rev. Lett.* **1983**, *50*, 1595−1598.
(13) Maple, M. B.; Chen, J. W.; Dalichaouch, Y.; Kohara, T.; Rossel, C.; Torikachvili, M. S.; McElfresh, M. W.; Thompson, J. D. *Phys. Rev. Lett.* **1986**, *56*, 185−188.
(14) Geibel, C.; Ahlheim, U.; Bredl, C. D.; Diehl, J.; Grauel, A.; Helfrich, R.; Kitazawa, H.; Kohler, R.; Modler, R.; Lang, M.; Schank, C.; Thies, S.; Steglich, F.; Sato, N.; Komatsubara, T. *Physica C* **1991**, *185*, 2651−2652.
(15) Ruderman, M. A.; Kittel, C. *Phys. Rev.* **1954**, *96*, 99−102.
(16) Kittel, C. *Introduction to Solid State Physics*; John Wiley & Sons: New York, 1996; p 628.

10.1021/ic060185w CCC: $33.50
Published on Web 05/11/2006

The coexistence of magnetism and superconductivity is quite unusual and, in fact, is magnetically mediated. Heavy fermion intermetallic compounds which show both magnetic ordering and superconductivity are of interest because they present the opportunity to study the competition or coexistence between the two mechanisms.

The crystal structure of $CeMIn_5$ (M = Co, Rh, Ir),[20,21] which adopts the $HoCoGa_5$-structure type,[22] consists of alternating layers of $CeIn_3$ and MIn_2 layers stacked along the *c* axis. Bulk $CeIn_3$ is a heavy fermion antiferromagnet which exhibits pressure-induced superconductivity. [23] $CeCoIn_5$ ($\gamma \approx 290$ mJ/mol of Ce K^2,)[24] under ambient conditions, has the highest superconducting transition temperature ($T_c = 2.3$ K) reported for any heavy fermion compound.[18] The magnetization of $CeCoIn_5$ is highly anisotropic, exhibiting a weak metamagnetic transition around 4.2 T along the *c* axis, while it gradually increases along the *a*−*b* plane.[25] $CeRhIn_5$ orders antiferromagnetically at $T_N = 3.8$ K and becomes superconducting at 2 K upon the application of >16 kbar of pressure with a $\gamma \approx 420$ mJ/mol of Ce K^2.[18] $CeIrIn_5$, under ambient conditions, has the largest Sommerfeld coefficient for the series with $\gamma \approx 750$ mJ/mol of Ce K^2.[26] The superconducting temperature of $CeIrIn_5$ is 0.4 K, however there is a resistivity drop at 1.2 K, of which there is debate about the mechanism responsible for the decrease in resistivity.[18] Upon the application of pressure, the transition temperature at 0.4 K increases to a maximum value of ~1 K at approximately 15 kbar. The highest ordering temperatures reported for this class of compounds are those observed in $GdRhIn_5$ and $GdIrIn_5$ which order antiferromagnetically at Néel temperatures of 40 and 42 K, respectively.[27,28] Reduced spatial dimensionality and magnetic anisotropy, as a function of the rare-earth element, have been observed in $LnRhIn_5$ (Ln = Ce, Nd, Sm, Gd). In an effort to further study the effects of magnetic anisotropy in Kondo systems, we were prompted to study $TbRhIn_5$. In this manuscript we compare the structure, transport, and physical properties of single crystals of $TbRhIn_5$ with other magnetic analogues, $CeRhIn_5$, $SmRhIn_5$, $NdRhIn_5$, and $GdRhIn_5$.

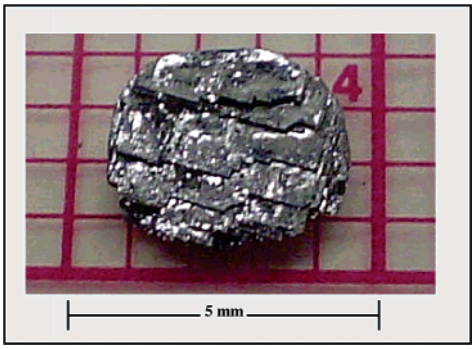

Figure 1. Aggregate of $TbRhIn_5$ (~4 mm).

Table 1. Crystallographic Parameters of $TbRhIn_5$

a (Å)	4.6000(6)
c (Å)	7.4370(11)
V (Å^3)	157.29(6)
cryst syst	tetragonal
Z	1
cryst dimension (mm^3)	0.075 × 0.025 × 0.025
space group	*P*4/*mmm*
θ range (deg)	2.5−30.0
μ (mm^{-1})	31.481
measured refls	742
independent reflns	244
reflns with $I > 2\sigma(I)$	163
R_{int}	0.097
h, *k*, *l*	±7, ±5, ±11
[a]R1 [$F^2 > 2\sigma(F^2)$]	0.0432
[b]wR2 (F^2)	0.0833
params	12
$\Delta\rho_{max}$(e Å^{-3}), $\Delta\rho_{min}$(e Å^{-3})	3.24, −4.52
extinction coeff	0.0066(7)

[a] $R1 = \Sigma||F_o| - |F_c||/\Sigma|F_o|$. [b] $wR2 = [\Sigma[w(F_o^2 - F_c^2)^2]/\Sigma[w(F_o^2)^2]]^{1/2}$.

Experimental Section

Synthesis. Tb pieces, Rh powder, and In shot (Alfa Aesar), all with stated purities of ≥99.9%, were combined in an atomic ratio of 1:1:20. The starting materials were then placed into an alumina crucible and sealed in an evacuated fused silica tube. The sealed sample was then gradually heated from room temperature to 1373 K at a rate of 473 K/h for 2 h, then slowly cooled at 281 K/h to 923 K, at which point the excess flux was removed via centrifugation. Synthesis yielded aggregates of layered crystals exhibiting a metallic luster as shown in Figure 1.

Single-Crystal X-ray Diffraction. A 0.025 × 0.025 × 0.075 mm^3 single-crystal fragment was placed on a glass fiber and mounted on the goniometer of a Nonius Kappa CCD diffractometer equipped with Mo Kα radiation ($\lambda = 0.71073$ Å). Data were collected at 293(2) K. Additional data collection and crystallographic parameters are presented in Table 1.

The structures were solved with the SHELXL software package[29] using $CeRhIn_5$ as a structural model. The atomic displacement parameters were treated anisotropically, and an extinction coefficient was applied to the data after a final least-squares cycle. The atomic coordinates and displacement parameters are provided in Table 2, and selected interatomic distances are listed in Table 3.

(17) Haga, Y.; Inada, Y.; Harima, H.; Oikawa, K.; Murakawa, M.; Nakawaki, H.; Tokiwa, Y.; Aoki, D.; Shishido, H.; Ikeda, S.; Watanabe, N.; Onuki, Y. *Phys. Rev. B* **2001**, *63*, 060503.
(18) Petrovic, C.; Pagliuso, P. G.; Hundley, M. F.; Movshovich, R.; Sarrao, J. L.; Thompson, J. D.; Fisk, Z.; Monthoux, P. *J. Phys.: Condes. Matter* **2001**, *13*, L337−L342.
(19) Petrovic, C.; Movshovich, R.; Jaime, M.; Pagliuso, P. G.; Hundley, M. F.; Sarrao, J. L.; Fisk, Z.; Thompson, J. D. *Europhys. Lett.* **2001**, *53*, 354−359.
(20) Kalychak, Y. M.; Zaremba, V. I.; Baranyak, V. M.; Bruskov, V. A.; Zavalii, P. Y. *Russ. Metall.* **1989**, *1*, 213−215.
(21) Moshopoulou, E. G.; Fisk, Z.; Sarrao, J. L.; Thompson, J. D. *J. Solid State Chem.* **2001**, *158*, 25−33.
(22) Grin, Y. N.; Yarmolyuk, Y. P.; Gradyshevsky, E. I. *Z. Kristallogr.* **1979**, *24*, 242−246.
(23) Mathur, N. D.; Grosche, F. M.; Julian, R. S.; Walker, I. R.; Freye, D. M.; Haselwimmer, K. W.; Lonzarich, G. G. *Nature* **1998**, *394*, 39−43.
(24) Stadelmaier, H. H.; Schobel, J. D.; Jones, R. A.; Shumaker, C. A. *Acta Crystallogr.* **1973**, *29*, 2926−2929.
(25) Murphy, T. P.; Hall, D.; Palm, E. C.; Tozer, S. W.; Petrovic, C.; Fisk, Z.; Goodrich, R. G.; Pagliuso, P. G.; Sarrao, J. L.; Thompson, J. D. *Phys. Rev. B.* **2002**, *65*, 100514.
(26) Hegger, H.; Petrovic, C.; Moshopoulou, E. G.; Hundley, M. F.; Sarrao, J. L.; Fisk, Z.; Thompson, J. D. *Phys. Rev. Lett.* **2000**, *84*, 4986−4989.
(27) Pagliuso, P. G.; Thompson, J. D.; Hundley, M. F.; Sarrao, J. L.; Fisk, Z. *Phys. Rev. B* **2001**, *63*, 054426.
(28) Latka, K.; Kmiec, R.; Rams, M.; Pacyna, A. W.; Zaremba, V. I.; Pottgen, R. *Z. Naturforsch. B* **2004**, *59*, 947−957.
(29) Sheldrick, G. M. *SHELXL97*; University of Göttingen: Göttingen, Germany 1997.

Table 2. Atomic Positions and Thermal Parameters of $TbRhIn_5$

		x	*y*	*z*	U_{eq}[a] (Å^2)
Tb	1a	0	0	0	0.014(3)
Rh	1b	0	0	1/2	0.015(2)
In1	4i	1/2	1/2	0	0.018(4)
In2	1c	0	1/2	0.3015(8)	0.017(3)

[a] U_{eq} is defined as one-third of the trace of the orthogonalized $\boldsymbol{U}_{ij}$ tensor.

Table 3. Selected Interatomic Distances (Å) and Bond Angles (deg) of $TbRhIn_5$

within cuboctahedra	
In1−In2	3.2140(12)
In1−In1	3.2527(4)
Tb−In1 (×4)	3.2140(12)
Tb−In2 (×8)	3.2527(4)
In1−Tb−In1	90
In1−Tb−In2	60.960(8)
In1−Tb−In2	119.040(8)
In2−Tb−In2	88.330(2)
In2−Tb−In2	59.520(4)
In2−Tb−In2	120.480(4)
within rectangular polyhedron	
In2−In2 (*c* axis)	2.9470(3)
In2−In2 (*a*−*b* plane)	3.2562(7)
Rh−In2 (×8)	2.7316(9)
In2−Rh−In2	73.130(13)
In2−Rh−In2	65.200(2)

Physical Property Measurements. Magnetic properties were measured on single crystals using a Quantum Design (SQUID) magnetometer. The temperature-dependent susceptibility was measured in an applied field of 1000 G up to room temperature after being cooled to 2 K under zero magnetic field. Field-dependent magnetization data were also collected from zero field to 10 T at 2 K. The resistivity (down to 2 K) data were measured using a standard four-probe method with a Quantum Design physical property measurement system (PPMS) at ambient pressure. Specific heat data was determined using the thermal transport option on the PPMS. The heat capacity of the $TbRhIn_5$ was measured at zero field in the temperature range of 300−0.36 K. Single crystals of the nonmagnetic analogue, $LaRhIn_5$ which were used for heat capacity measurements, were also grown using the flux method at Los Alamos National Lab (LANL).

Results and Discussion

$TbRhIn_5$ is isostructural to the $CeMIn_5$ (M = Co, Rh, Ir) compounds which adopt the $HoCoGa_5$-type structure (*P*4/*mmm*).[22] The structure consists of four atoms in the asymmetrical unit: Tb, Rh, In1, and In2 atoms occupying the 1a, 1b, 1c, and 4i Wycoff positions, respectively. Figure 2 shows the crystal structure of $TbRhIn_5$ which consists of alternating layers of $TbIn_3$ cuboctahedra and $RhIn_2$ rectangular prisms that contain two independent indium sites, In1 and In2. The coordination of Tb in the cuboctahedra is 8-fold to In1 and 4-fold to In2 with distances of 3.2140(12) and 3.2527(4) Å, respectively. These distances are in good agreement with the Tb−In interatomic distances in the binary compounds, Tb_2In and $TbIn_3$, in which the Tb−In distances range from 3.025 to 3.359 Å.[30]

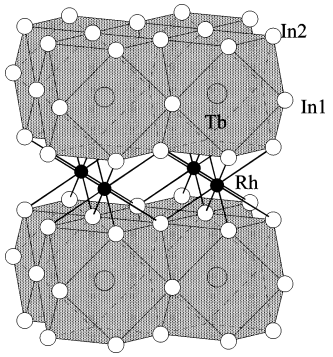

Figure 2. Structure of $TbRhIn_5$ consisting of layers of $TbIn_3$ cuboctahedra (gray). alternating with layers of $RhIn_2$, in which the Rh and In atoms are designated as black and white closed circles, respectively.

In $CeCoIn_5$, the cuboctahedra are elongated along the *c* axis, while a shortening of the *c* axis is observed in the Ir analogue. The ratio of Ce−In2/Ce−In1 in $CeRhIn_5$ is close to unity, indicating that the cuboctahedra are not distorted.[31] The ratio of Tb−In2/Tb−In1 is 1.014, suggesting that the cuboctahedra in $TbRhIn_5$ are quite symmetrical.

The Rh atom is coordinated to eight In2 atoms and forms the edge of the neighboring rectangular prism. The Rh−In2 distance in $TbRhIn_5$ is 2.7316(9) Å and is comparable to the Rh−In2 distances of 2.7572(3) Å observed in $LaRhIn_5$, as well as the summation of the atomic radii for rhodium and indium.[31] The In1−In2 and In1−In1 interatomic distances in $TbRhIn_5$ are 3.2140 (12) and 3.2527(4) Å, respectively, which are in good agreement with the values observed in RhIn[32] and $RhIn_3$,[33,34] ranging from 3.200 to 3.580 Å.

Physical Properties. The temperature dependence of the magnetic susceptibility of $TbRhIn_5$ is shown in Figure 3 for the field (1000 G) both along the *c* axis and in the *a*−*b* plane. A large anisotropy in the susceptibility data is observed. A sharp antiferromagnetic transition appears at 48 K. Above T_N, the inverse susceptibility obeys the Curie−Weiss law and is well fit by $[1/\chi(T) = (T - \theta)/C]$ in the temperature range of 80−300 K. We find an average effective moment of ∼9.72 μ_B/Tb^{3+} ion along the *c* axis and the *a*−*b* plane with Weiss temperatures of $\theta = -75$ and −5 K, respectively. The effective moment is in agreement with the full Hund's moment for Tb^{3+} which is 9.72 μ_B. The negative θ values indicate antiferromagnetic correlations, which are quite strong along the *c* axis.

Figure 4 shows the field-dependent magnetization of $TbRhIn_5$ at 2 K along the *c* axis and the *a*−*b* plane up to 7 T. The magnetization increases with field up to 7 T with induced moments at the maximum field equal to 1.18 and 0.88 μ_B for the *c* axis and *a*−*b* plane, respectively, indicating

(30) Bazela, W.; Szytula, A. *J. Less-Common Met.* **1988**, *138*, 123−128.
(31) Macaluso, R. T.; Sarrao, J. L.; Pagliuso, P. G.; Moreno, N. O.; Goodrich, R. G.; Browne, D. A.; Fronczek, F. R.; Chan, J. Y. *J. Solid State Chem.* **2002**, *166*, 245−250.
(32) Schubert, K.; Breimer, H.; Burkhardt, W.; Gunzel, E.; Haufler, R.; Lukas, H.; Vetter, H.; Wegst, J.; Wilkens, M. *Naturwissenschaften* **1957**, *44*, 229−233.
(33) Schubert, K.; Lukas, H.; Meissner, H.; Bhan, S. *Z. Metallkunde* **1959**, *50*, 534−540.
(34) Pöttgen, R.; Hoffmann, R. D.; Kotzyba, G. *Z. Anorg. Allg. Chem.* **1998**, *624*, 244−250.

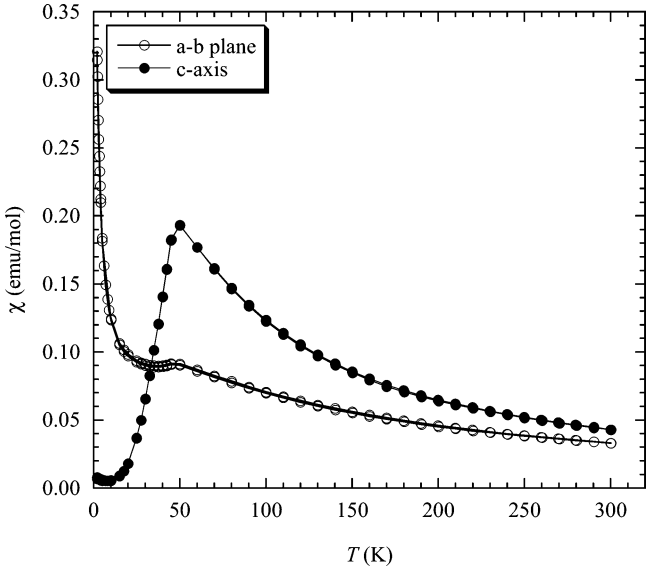

Figure 3. Temperature-dependent magnetic susceptibility (χ) of $TbRhIn_5$ along the $a-b$ plane (open circles) and c axis (closed circles) measured at 1000 G.

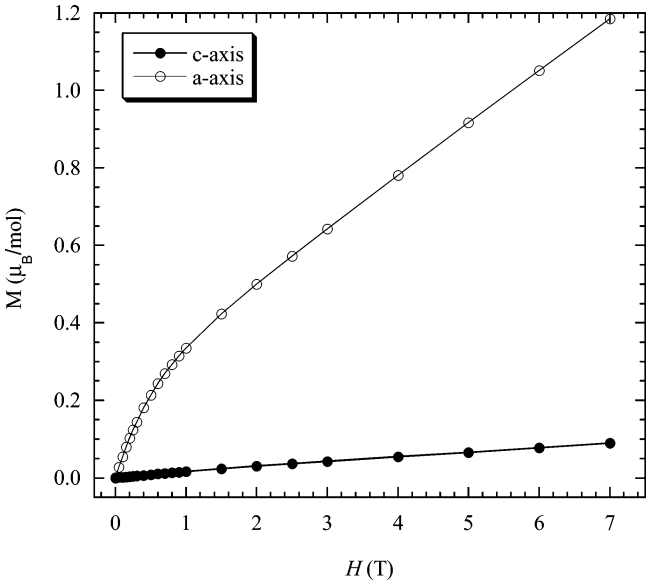

Figure 4. Field-dependent magnetization of $TbRhIn_5$ along the $a-b$ plane (open circles) and c axis (closed circles) measured at 2 K.

that 7 T is not a significant field to induce saturation of the magnetic moments in $TbRhIn_5$. These values are significantly smaller than the full Hund's saturation moment of 9 μ_B expected for a Tb^{3+} ion.

The temperature dependence of the electrical resistivity of a single crystal of $TbRhIn_5$ is shown in Figure 5. $TbRhIn_5$ is metallic ($d\rho/dT > 0$) and has a residual resistivity ratio (RRR) of 6. A kink in the resistivity is observed near the ordering temperature at 48 K, consistent with a reduction in the spin-disorder scattering. Above T_N, the resistivity increases linearly with temperature. The small downturn at 3.4 is caused by some residual In flux in the sample.

Figure 6 shows the temperature dependence of the specific heat, C_p, for $TbRhIn_5$. At zero field, a large cusp is observed at ~48 K which is consistent with the antiferromagnetic transition observed in the susceptibility. The specific heat

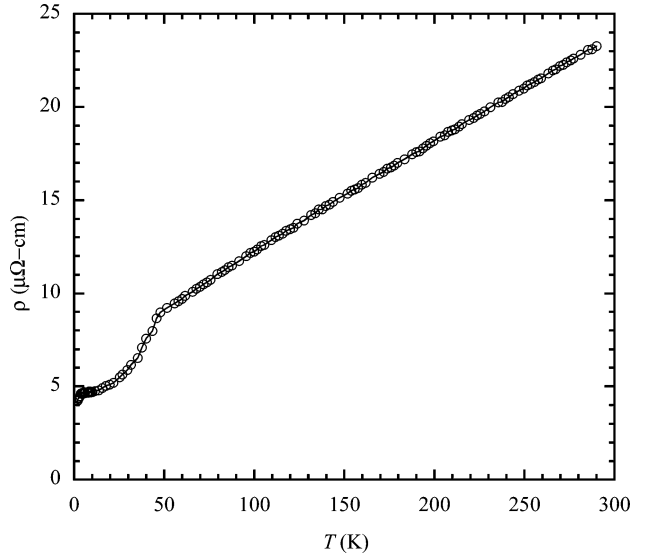

Figure 5. Temperature-dependent resistivity of $TbRhIn_5$.

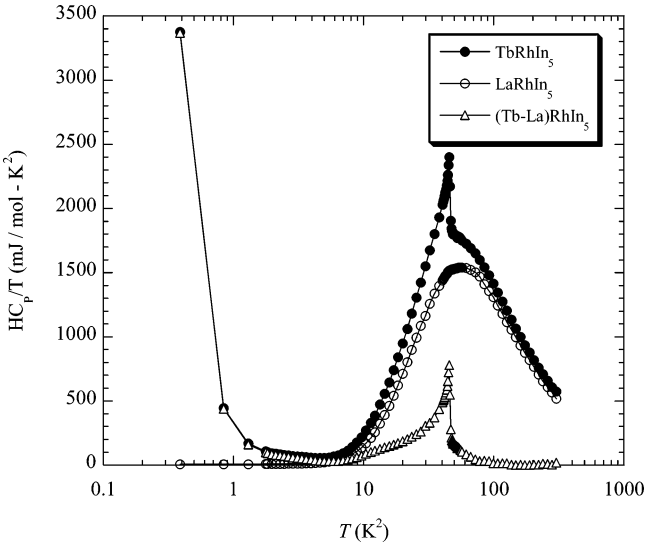

Figure 6. Specific heat of $TbRhIn_5$ (closed circles) and $LaRhIn_5$ (open circles). The f electron contribution of Tb is denoted with open triangles.

can be described by the equation $C_p = \gamma T + \alpha T^3$, where γ is the Sommerfeld coefficient and α is the phonon contribution to the total specific heat. The phonon contribution is negligible at low temperatures, which allows the electronic contribution to the specific heat to be determined experimentally. The f electron contribution to the specific heat, C/T_m (Figure 6), is obtained by subtracting the phonon contribution C/T of $LaRhIn_5$. Since $LaRhIn_5$ does not contain any f electrons, it is a good approximation of the lattice contribution to the specific heat. The specific data in $TbRhIn_5$ is similar to other antiferromagnetic $LnMIn_5$ materials. Several mechanisms act simultaneously to produce the specific heat data as shown in Figure 6. There is a large nuclear Schottky contribution at low temperatures (below 2K). It results from the hyperfine interaction between the 4f electrons and the Tb^{3+} nuclei, which carry a nuclear spin moment of $I = 3/2$. There is a possible Schottky anomaly resulting from the crystalline electric field (CEF) at 11 K as shown in Figure 7, and there is a large peak at 48 K from

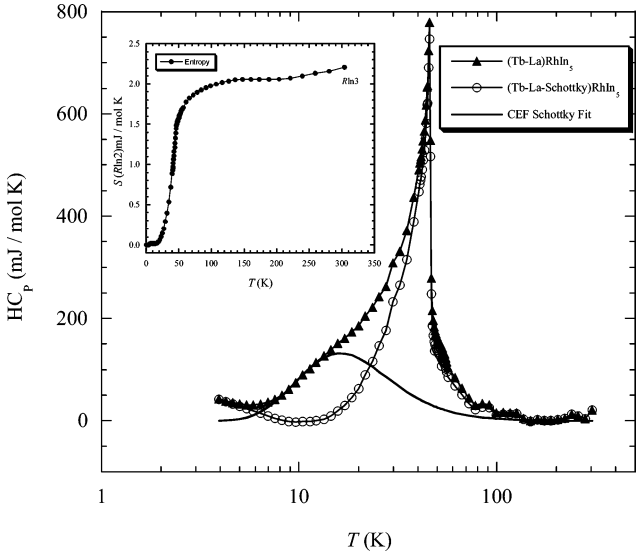

Figure 7. Specific heat of TbRhIn$_5$ after subtracting the lattice contribution (closed triangles), Schottky (line), and nuclear Schottky contributions (open circles). The entropy of TbRhIn$_5$ is shown in the inset.

the antiferromagnetic transition. The entropy is obtained by integrating C/T_m with respect to temperature. A value of R ln 3 is recovered by the ordering temperature. Since the number of states, N, is determined by the entropy as R ln N, this confirms that Tb is in a triplet ground state ($N = 3$).

In summary, TbRhIn$_5$ has been synthesized using flux methods and is isostructural to the well-studied CeRhIn$_5$. The magnetic moments of CeRhIn$_5$ form an incommensurate spiral along the c axis,[26,35] and although CEF anisotropy energetically favors the moments to point along the c axis, the magnetic moments have been found to lie in the $a-b$ plane.[36] Thus there may be competition between the two magnetic interactions, since we observe a 50% decrease in T_N for CeRhIn$_5$ in comparison to the parent compound CeIn$_3$. In contrast, the easy axis of magnetization in TbRhIn$_5$ ($T_N = 47$ K) is along the c axis; therefore, T_N is enhanced nearly 24% compared to that in TbIn$_3$ ($T_N = 36$ K).[37] In addition, the enhanced T_N indicates that RKKY interactions are more dominant than the Kondo effect in this compound because we observe more interaction between the uncompensated rare-earth ions. The magnetic susceptibility of GdRhIn$_5$ is only significantly anisotropic below T_N showing an easy axis of magnetization in the plane. Furthermore, CeRhIn$_5$ becomes superconducting under 16 kbar of mechanical pressure, but the superconducting state diminishes at ~25 kbar. The size of the atomic radii of Ce^{3+} versus Tb^{3+} decreases by ~3.4% because of lanthanide contraction. Multiplying 16 kbar by 3.4% gives an estimated molecular pressure for TbRhIn$_5$ of ~25 kbar, at which point the superconducting state diminishes in CeRhIn$_5$.[21] The magnetic-ordering temperature of TbRhIn$_5$ scales in accordance with the de Gennes factor $[(g_J^2 - 1)][J(J + 1)]$ of LnRhIn$_5$ (Ln = Ce, Nd, Sm, Gd) for a ground-state multiplet, J, through the rare earths, with a T_N of 3.8−48 K for the Ce and Tb analogues. Although TbRhIn$_5$ is not a heavy fermion superconductor, it does have strong antiferrromagnetic correlations resulting in an ordering temperature much higher than its heavy fermion analogue CeRhIn$_5$. It would be interesting to do a doping study by substituting Ce for Tb in TbRhIn$_5$ to observe how the heavy fermion superconducting state develops out of a strong antiferromagnet.

Acknowledgment. Z.F and D.P.Y. thank the NSF for financial support (DMR 0503361 and DMR 0449022, respectively). J.Y.C. acknowledges the NSF Career (DMR 0237664) and Alfred P. Sloan Fellowship for partial support of this project.

Supporting Information Available: Crystallographic data in CIF format. This material is available free of charge via the Internet at http://pubs.acs.org.

IC060185W

(35) Pagliuso, P. G.; Curro, N. J.; Moreno, N. O.; Hundley, M. F.; Thompson, J. D.; Sarrao, J. L.; Fisk, Z. *Physica B* **2002**, *320*, 370−375.

(36) Bao, W.; Pagliuso, P. G.; Sarrao, J. L.; Thompson, J. D.; Fisk, Z.; Lynn, J. W.; Erwin, R. W. *Phys. Rev. B* **2001**, *6321*, 219901.

(37) Buschow, K. H. J. *J. Chem. Phys.* **1968**, *50*, 137−141.